Article

Molecular Dynamics Analysis of Antibody Recognition and Escape by Human H1N1 Influenza Hemagglutinin

Pek Ieong,[1] Rommie E. Amaro,[1,*] and Wilfred W. Li[2,*]

[1]Department of Chemistry and Biochemistry and [2]San Diego Supercomputer Center, University of California San Diego, La Jolla, California

ABSTRACT   The antibody immunoglobulin (Ig) 2D1 is effective against the 1918 hemagglutinin (HA) and also known to cross-neutralize the 2009 pandemic H1N1 influenza HA through a similar epitope. However, the detailed mechanism of neutralization remains unclear. We conducted molecular dynamics (MD) simulations to study the interactions between Ig-2D1 and the HAs from the 1918 pandemic flu (A/South Carolina/1/1918, 18HA), the 2009 pandemic flu (A/California/04/2009, 09HA), a 2009 pandemic flu mutant (A/California/04/2009, 09HA_mut), and the 2006 seasonal flu (A/Solomon Islands/3/2006, 06HA). MM-PBSA analyses suggest the approximate free energy of binding (ΔG) between Ig-2D1 and 18HA is -74.4 kcal/mol. In comparison with 18HA, 09HA and 06HA bind Ig-2D1 ~6 kcal/mol ($\Delta\Delta G$) weaker, and the 09HA_mut bind Ig-2D1 only half as strong. We also analyzed the contributions of individual epitope residues using the free-energy decomposition method. Two important salt bridges are found between the HAs and Ig-2D1. In 09HA, a serine-to-asparagine mutation coincided with a salt bridge destabilization, hydrogen bond losses, and a water pocket formation between 09HA and Ig-2D1. In 09HA_mut, a lysine-to-glutamic-acid mutation leads to the loss of both salt bridges and destabilizes interactions with Ig-2D1. Even though 06HA has a similar ΔG to 09HA, it is not recognized by Ig-2D1 in vivo. Because 06HA contains two potential glycosylation sites that could mask the epitope, our results suggest that Ig-2D1 may be active against 06HA only in the absence of glycosylation. Overall, our simulation results are in good agreement with observations from biological experiments and offer novel mechanistic insights, to our knowledge, into the immune escape of the influenza virus.

INTRODUCTION

Influenza virus gains entry into the human body through interactions of the viral surface glycoproteins called hemagglutinin (HA) with the sialic acid (Sia) receptors on the human epithelial cell surface (1,2). Sia is found at the terminals of glycans attached covalently to cell surface glycoproteins or glycolipids. They are also found on the viral surface proteins (3). During viral infection, viral HA binds to Sia receptors on human host cells, and the virus enters through endocytosis. The flu virus then usurps host cell machineries for viral replication (4). There are 18 known HA serotypes: H1 to H18. Among these serotypes, H1 and H5 are the most extensively studied. H1 is found to bind preferentially to Sia with an α-2,6 glycosidic bond, whereas H5 prefers Sia with α-2,3 linkage (5).

Humans fight influenza infection through innate and adaptive immune responses (6) including vaccination or use of pharmaceutical drugs such as Tamiflu or Relenza (7). The adaptive immune response involves the recognition of HA epitopes by human immune cells and the production of antibodies against HA. Inactivated, live attenuated virus or recombinant HA are often prepared as vaccines, which elicit antibody production 7 days after inoculation (8). Antibodies bind HA epitopes, preventing Sia binding and endocytosis (9). Four main canonical epitopes on the globular HA head have been identified: Sa, Ca, Sb, and Cb (Fig. 1) (10,11). More recently, cross-reacting antibodies against multiple HA subtypes have been discovered that target the globular epitopes and the conserved stem regions (12–14). Preexisting antibodies from vaccination or earlier infections may prevent infection by viral strains with similar HA epitopes (8,15).

Influenza viruses avoid human immune responses through antigenic drift and antigenic shift. In antigenic drift, mutations in glycoprotein epitopes render existing antibodies ineffective, a process facilitated by the high mutation rate of the influenza RNA genome (16). As a result, annual vaccines may offer partial protection or fail completely against unanticipated strains. In antigenic shift, abrupt changes in viral RNA genome result when several different viral strains recombine, creating a hybrid virus. The resulting virus is novel and distinctive, to our knowledge, sometimes posing lethal threats to the human population. The 2009 swine flu, which emerged from a triple assortment involving swine, human, and avian reservoirs, is a good example (17). Since it first appeared in the human population in April 2009, it quickly spread globally and was declared pandemic by the World Health Organization in June 2009 (18).

A   Sequence Alignment

Canonical epitope

Surrounding epitope residues

```
                130       140       150       160       170       180
2006HA  FPKESSWPNHTT-TGVSASCSHNGESSFYKNLLWLTGKNGLYPNLSKSYANNKEKEVLVL
1918HA  FPKTSSWPNHETTKGVTAACSYAGASSFYRNLLWLTKKGNSYPKLSKSYVNNKGKEVLVL
2009HA  FPKTSSWPNHDSNKGVTAACPHAGAKSFYKNLIWLVKKGNSYPKLSKSYINDKGKEVLVL
2009HA_mut  FPKTSSWPNHDSNKGVTAACPHAGAKSFYKNLIWLVKKGNSYPKLSESYINDKGKEVLVL

                190       200       210       220       230       240
2006HA  WGVHHPPNIGDQRALYHTENAYVSVVSSHYSRKFTPEIAKRPKVRDREGRINYYWTLLEP
1918HA  WGVHHPPTGTDQQSLYQNADAYVSVGSSKYNRRFTPEIAARPKVRDQAGRMNYYWTLLEP
2009HA  WGIHHPSTSADQQSLYQNADTYVFVGSSRYSKKFKPEIAIRPKVRDQEGRMNYYWTLVEP
2009HA_mut  WGIHHPSTSADQQSLYQNADTYVFVGSSRYSKKFKPEIAIRPKVRDQEGRMNYYWTLVEP

                250       260       270       280       290       300
2006HA  GDTIIFEANGNLIAPRYAYAFALSRGFGSGIINSSNAPMDECDAKCQTPQGAINSSLPFQNVH
1918HA  GDTITFEATGNLIAPWYAFALNRGSGSGIITSDAPVHDCNTKCQTPHGAINSSLPFQNIH
2009HA  GDKITFEATGNLVVPRYAFAMERNAGSGIIISDTPVHDCNTTCQTPKGAINTSLPFQNIH
2009HA_mut  GDKITFEATGNLVVPRYAFAMERNAGSGIIISDTPVHDCNTTCQTPKGAINTSLPFQNIH
```

B   Epitope Residues

a) S160

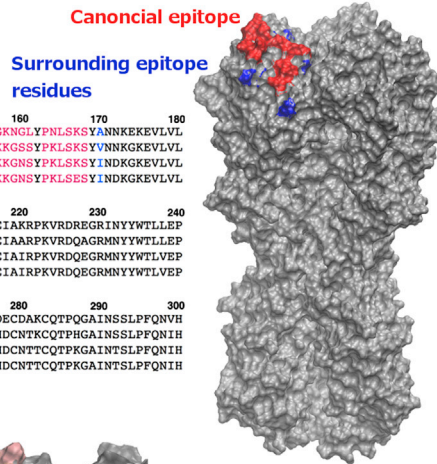b) N129   N164

c) N160   K167

d) E167

FIGURE 1 Sequence alignment and the epitopes of the four HA glycoprotein. (*A*) Sequence alignment and structural view. The four HA sequences are aligned and numbered using the 18HA numbering convention. On the right, the Sa epitope is colored red and the surrounding residues that form contact with Ig-2D1 (12) are colored blue (*top left*) in 18HA monomer 1. (*B*) Structural conservation of the HA epitope region and key mutations that affect antibody recognition. The four HAs are shown: (*a*) 18HA, (*b*) 06HA, (*c*) 09HA, and (*d*) 09HA_mut. The epitope residues on monomer 1 are colored by residue names. Several key residues are also labeled to their corresponding residue colors. S160 (18HA) is mutated in N160 in 09HA. K 167 (09HA) is mutated to E167 in 09HA_mut. N129 and N164 in 06HA are potential glycosylation sites. To see this figure in color, go online.
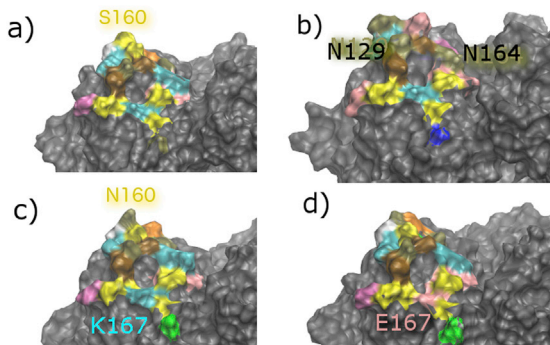
Although the elderly are particularly susceptible to seasonal flu, few from this age group have been infected by the 2009 pandemic strain (19). Some researchers have hypothesized that the elderly may be immune because of childhood exposure to the 1918 pandemic flu virus (18HA). The 09HA is found to be very similar, genetically and structurally, to the 18HA. Therefore, it is possible that antibodies that recognize the 18HA may also recognize the 09HA (12,20). Krause et al. showed that monoclonal immunoglobulin (Ig-2D1) against the 18HA appeared to cross-react with the 09HA from the pandemic flu (14).

To identify specific mutations that might affect HA binding, Liu et al. used computational methods to predict hotspot residues on the epitopes of the 09HA, 18HA, and 07HA from a 2007 seasonal strain (07HA) that interacts with Ig-2D1 (21). They suggested that mutations in the 18HA and 09HA at residues P128, N129, K158, P163, K164, and K167 (using 18HA numbering) could disable Ig-2D1 neutralization. Because N160 was not predicted as a hot-spot residue, Liu et al. proposed that a mutation from S160 in the 18HA to N160 in the 09HA would not affect binding. Their analysis of the binding between Ig-2D1 and the various HAs was performed on crystal structures, and protein flexibility was not considered explicitly.

In this article, we present new findings, to our knowledge, using molecular dynamics (MD) simulation in four influenza H1N1 systems of Ig-2D1 and HAs: A/South Carolina/1/1918, A/California/04/2009, A/Solomon Island/ 3/2006, and A/California/04/2009 mutant. We explore the underlying molecular interactions that govern Ig-2D1/HA binding to determine how Ig-2D1 is able to elicit a cross-reactive immune response to the 2009 influenza virus. Our results are in good agreement with previous experimental and computational studies. Additionally, we discovered that mutations such as the S160N mutation in 09HA do affect the stability of the antibody-antigen interaction.

MATERIALS AND METHODS

Simulation setup

The structures of the 06HA, 09HA, and 18HA were obtained from the Protein Data Bank (PDB) (12,22) with PDB ID 3SM5, 3LZG, and 3LZF, respectively. Only the 18HA was co-crystallized with Ig-2D1 (12). Seasonal strain HA and 09HA were superimposed on the 18HA structure to model Ig-2D1 binding to these HA variants. The numbering scheme for Ig-2D1 was adapted from the PDB structure. The trimeric units of HA were built after the superimposition according to the biological unit (23). The 09HA_mut and 09HA model differ by one single residue at position 167. It was prepared from the 09HA system by mutating the residue from K to E (K167E) using Schrödinger (24).

Molecular dynamics simulation

Four systems (18HA, 09HA, 06HA, and 09HA_mut) were parameterized with the Amber ff99SB force field (25). The systems were first neutralized by adding sodium ions. Additional ions were then added to achieve 20 mM NaCl buffer salt concentration. Histidine charges were assigned using

PROPKA from the pdb2pqr web server at pH 7.0 (26,27). Each system was solvated in a water box of ~150 × 160 × 210 Å using the TIP3P (28) water model. Each system had a total of ~500,000 atoms (Table S1 in the Supporting Material). MD simulations were performed afterward using NAMD 2.9 (29).

The systems were constrained and gradually minimized to reduce the total potential energy in a series of four steps of energy minimization. The first step kept all heavy atoms constrained, and only hydrogen atoms were allowed to fluctuate. The second step released the constraints on water and ions. The third steps freed the side chains. In the fourth step, all atoms were allowed to move without restriction. The nonbonded energy was calculated every two time steps with a cutoff distance of 12 Å. A switching function was applied at 10 Å to abridge the van der Waals potential function.

After minimization, four steps of equilibration were performed, gradually loosening harmonic constraints in 500 ps increments, for a total equilibration time of 2 ns. The first step heated the system to 310 K while applying a force of 4 kcal/mol to hold the backbone in place. The remaining three steps gradually lifted the backbone constraint force from 4 kcal/mol to 1 kcal/mol. NPT ensemble was completed. Langevin Dynamic was applied to keep the temperature constant throughout the equilibration, with a damping frequency of 5 ps/THz, and Langevin Priston barostat helped maintain the specified one atmospheric pressure. The constraints applied during equilibration were removed for the free simulation of the antigen-antibody complexes. All simulations were run for 69 ns using the XSEDE resources *Ranger*, *Stampede*, (both at TACC) and *Gordon* (SDSC).

Determining bond interactions

Barlow and Thornton proposed that salt bridges should be between oppositely charged residues ≤4.0 Å (30). Xu et al. reported that three salt bridges were found between the antigen-antibody interfaces in their Ig-2D1 and 18HA co-crystal structure (12). K158 interacts with the Ig heavy chain (IgH) D52 and D54, forming two distinct salt bridges, with bond distances of 3.7 Å and 3.0 Å, respectively. Additionally, K167 interacts with D93 on the Ig light chain (IgL) with a bond distance of 2.8 Å. For the purpose of this investigation, we defined a salt bridge to be between a pair of oppositely charged groups that contain at least one hydrogen bond within 3.5 Å of each other, as suggested by other researchers (31). This is because the H-bond may be important in the stability of salt bridges (31), as also supported later in this article.

We used the Visual Molecular Dynamics (VMD) software package (32) to analyze simulation trajectories. Xu et al. proposed a list of 18HA residues that interacted with Ig-2D1 (12). All reported interactions between Ig-2D1 and the different HAs were determined carefully based on atomic characteristics and a distance matrix. They included hydrogen bonds, salt bridges, and dipole-dipole and van der Waals interactions (e.g., Fig. S1). The distances between contacting atoms were recorded every 100 ps. The distance cutoffs were ≤3.5 Å for hydrogen bonds, ≤3.5 Å for salt bridges, and 2.6–4.6 Å for dipole-dipole interactions and van Del Waal interactions. To account for system dynamics and to capture the stability of the interactions, we calculated an interaction percentage using the distance matrix for each contact made between epitope residues and Ig-2D1. Only interactions present in at least two of the three monomers for 75% or more of the simulation time were considered important for the binding of HAs and Ig-2D1. Similarly, surrounding residues near the reported Sa epitope were also analyzed to identify possible contacts with Ig-2D1 found through simulation that had not been reported previously.

Free energy of binding and decomposition

The free energy of binding (ΔG) was approximated using the Molecular Mechanics–Poisson-Boltzmann Surface Area (MM-PBSA) method using MMPBSA.py implemented in AmberTools11 (33,34). The

Poisson-Boltzmann (PB) equation was utilized to estimate the polar contribution of the solvation energy. MMPBSA.py stripped the water molecules and ions and carried out the calculation in implicit solvent. The ionic strength for the free-energy calculation was also set to 20 mM. The receptor mask was set to the trimetric HA plus two Ig-2D1, and the ligand mask was always set to the remaining Ig-2D1. Thus, three free-energy calculations were performed to obtain the mean and standard error (SE) of ΔG for each system.

Per-residue free-energy decomposition was carried out to determine the energy contribution of epitope residues to the binding with Ig-2D1, using the MMPBSA.py tool from AmberTools13 (33,34). The Generalized Born (GB) implicit-solvent model was utilized for the decomposition calculation. Since GB was parameterized with the atomic radii mbondi2 (35), all the atom radii were changed from the default mbondi to mbondi2. Saltcon was also set to 20 mM. All other parameters were identical to those in AmberTools11. The decomposition analysis of individual residues was performed using igb2, not the default GB parameter (igb5). In a comparison of igb5 and igb2, we found that the ΔG calculated from igb2 was closer to the PB energy (data not shown). This result, consistent with that from our previous study, indicates that igb2 is well suited to the neuraminidase N1 and N9 systems (36).

RMSD and surface pocket volume calculations

UCSF Chimera was utilized to calculate the RMSD between crystal structures. Clustal Omega was applied to alignment the HA sequences (23,37). The POVME 2.0 software (38) was used to calculate the surface pocket volumes at the interface of HAs and Ig-2D1 near residue S/N160 in 18HA and 09HA. A 12 Å radius sphere was centered on the S/N160 center of mass fully covering S/N160 and surrounding Ig-2D1 residues. The volume calculations were done separately for each monomer, and an average was reported for each system. A cylinder (25 Å in radius and 4 Å tall) that fully encompassed the interface was used to calculate the volume between the antibody-antigen interface in the 09HA and 09HA_mut systems. The center of the cylinder was positioned at the center of mass of all epitope residues, and oriented toward (−1, 0, 4) for Ig1, (4, 1, 0) for Ig2, and (−1, 4, 0) for Ig3.

RESULTS

Structure and sequence alignments

The 18HA, 09HA, and 06HA selected in this study are structurally conserved (12), with RMSD values of 0.851 Å (09HA) and 0.927 Å (06HA), in comparison with the 18HA (Fig. 1). Of the 20 HA epitope residues known to interact with Ig-2D1 in the 18HA, two mutations were found in the 09HA and 10 mutations in the 06HA. As reported earlier, 06HA contained two glycosylation sites N129 and N164 (NxS/T, where *x* is any amino acid other than proline), because of an E131T mutation and a K164N mutation (Fig. 1) (22).

Bond interactions

In Table 1, we compare the number of bond interactions between HA epitope residues and Ig-2D1. The heavy and light chains of Ig-2D1 are indicated using IgH and IgL, respectively. Notably, from the single-point mutation from the 09HA to the 09HA_mut, three H-bonds between S126, K167, and S168 (09HA) and D93, N31, and S30 (IgL)

TABLE 1 Interactions between HA and Ig-2D1 systems categorized by bond types

	Salt Bridge	H-Bond	Dipole-Dipole	van der Waals
18HA	2	11	23	4
06HA	1	6	11	4
09HA	1	6	11	5
09HA_mut	0	4	11	5

H-bond stands for hydrogen bond. Dipole-dipole stands for dipole-dipole interactions. A salt bridge is formed between negatively and positively charged residues within 3.5Å of each other. The van der Waals force is the interaction between hydrophobic residues. More details are in Tables S2–S5. Table S2 also indicates interactions found in crystal structure only for 18HA.

were lost, respectively, whereas a new H-bond interaction was formed between Y162 (09HA_mut) and S99 (IgH). This is a net loss of two H-bonds between the 09HA and 09HA_mut.

In the 18HA, K158 and K167 form two distinct salt bridges with D54 (IgH) and D93 (IgL) in the Ig-2D1. These two lysine residues are conserved in all naturally occurring HAs (Fig. 1).

By contrast, the 09HA system has only one salt bridge (K167-D93). An earlier study by Krause et al. suggested that mutations of K167 in the 09HA to E or N (K167E/N) allow the 09HA to escape neutralization from monoclonal antibody Ig-2D1 (14). We recreated the 09HA_mut carrying the K167E mutation in silico, and the resulting mutant lost both salt bridges. Overall, the Ig-2D1 lost about half of the H-bond and dipole-dipole interactions in the 09HA and 09HA_mut systems compared with the original 18HA system. Together, these observations suggest that the Ig-2D1 may not bind as strongly to the more recent HAs because of loss of these interactions.

Free energy of binding calculation

The approximate average ΔG for each system was obtained using the MM-PBSA method (33). The 18HA had the lowest ΔG with respect to Ig-2D1 (Table 2) at -74.4 ± 1.1 kcal/mol. The 09HA and the 06HA systems were ~6 kcal/mol lower ($\Delta\Delta G$), with similar ΔG values of -68.0 ± 1.2 kcal/mol and -67.6 ± 1.6 kcal/mol, respectively (Table 2). The calculated ΔG values are consistent with the observed number of interaction shown in Table 1. Both the 09HA and 06HA had higher $\Delta\Delta G$s compared

with the 18HA by $+6.4 \pm 1.6$ kcal/mol and $+6.8 \pm 1.9$ kcal/mol, respectively. In contrast, the average ΔG of the 09HA_mut was significantly higher: $+36.5 \pm 1.9$ kcal/mol than that of 18HA. Compared with that of 09HA, the ΔG of the 09HA_mut system increased by $+30.1 \pm 2.0$ kcal/mol, even though the only difference was a K167E mutation in 09HA_mut. The 09HA_mut ΔG result is in agreement with the K167E escape mutant selected by Krause et al. (14). The MM-GBSA method also gave very similar results (Table 2).

Free-energy decomposition

To further study the contribution of each epitope residue and probe the importance of K167, we performed free-energy decomposition using MM-GBSA (Tables 3 and S8). The average ΔG of the binding-energy contribution from K167 was predicted to be -6.6 ± 0.2 kcal/mol in 18HA, the highest contribution of all the epitope residues. This is also true in the 09HA and 06HA systems: the ΔG of the binding-energy contributions of K167 are -6.3 ± 0.2 kcal/mol and -6.6 ± 0.2 kcal/mol, respectively. Krause et al. identified an escape mutation K167E that prevents Ig-2D1 from neutralizing 09HA (14). In the K167E 09HA_mut system, the free-energy decomposition results showed that this mutation was highly unfavorable, with a ΔG contribution of $+2.9 \pm 0.1$ kcal/mol (Table 3). The mutation increased the residue decomposition energy by $+9.2 \pm 0.3$ kcal/mol. Putting a negatively charged glutamic acid residue in the place of a positively charged lysine residue would lead to electrostatic repulsion with structural consequences on the HA-Ig2D1 complex.

Mechanistic insight from the 09HA immune escape mutation

During the minimization step of the 09HA_mut system, the complementarity-determining region (CDR) L3 loop containing D93 (IgL), the salt bridge partner with K167 (09HA), shifted away from E167 (09HA_mut) (Fig. 2). E167 (09HA_mut) then formed two hydrogen bonds interacting with S30 and N31 (IgL) in the CDR L1 loop. Initially, the CDR L1 loop maintained these hydrogen bonds (Fig. 2 A). Both the L1 and L3 loops had shifted away from E167 and the antigen at the end of the simulation (Fig. 2 B). The number of atoms within 4.6 Å of E167 from the CDR L1 and L3 loops dropped from 13 atoms to around 4 atoms as early as 3 ns into the simulation (Fig. 2 C). The movement

TABLE 2 Estimated ΔG free energy of binding for each system using MM-PB/GBSA

	18HA (N = 248)		06HA (N = 248)		09HA (N = 249)		09HA_Mut (N = 247)	
	Average	SE	Average	SE	Average	SE	Average	SE
PB $\Delta G_{subtotal}$	-74.4	1.1	-67.6	1.6	-68.0	1.2	-37.9	1.6
GB $\Delta G_{subtotal}$	-74.5	1.0	-63.4	1.5	-62.7	1.1	-39.1	1.1

N is the number of frames used in the calculation. Each frame is ~0.28 ns of the simulations. Average ΔG energy and standard error (SE) are calculated from three sample runs in each system. All values are in kcal/mol. Only $\Delta G_{subtotal}$ is reported. The individual components are reported in Tables S6 and S7.

TABLE 3 Free-energy decomposition of epitope residues in the four systems

Residue ID	18HA		06HA		09HA		09HA_mut	
	Residue	$\Delta G \pm SE$	Residue	$\Delta G \pm SE$	Residue	$\Delta G \pm SE$	Residue	$\Delta G \pm SE$
158	K	−4.4 ± 0.2	–	−2.2 ± 0.2	–	−2.3 ± 0.2	–	−1.9 ± 0.2
159	G	−3.1 ± 0.1	N	−2.9 ± 0.1	–	−2.2 ± 0.1	–	−1.8 ± 0.1
160	S	−4.9 ± 0.2	G	−0.0 ± 0.0	N	−0.5 ± 0.1	N	−0.9 ± 0.1
161	S	−1.8 ± 0.1	L	−4.0 ± 0.1	–	−1.8 ± 0.1	–	−2.0 ± 0.1
167	K	−6.6 ± 0.2	–	−6.6 ± 0.2	–	−6.3 ± 0.2	E	2.9 ± 0.1

Only selected key residues—158, 159, 160, 161, and 167—are shown. All epitope-residue-based decomposition results appear in the Supporting Material (Table S8). All units are in kcal/mol.

of the L1 and L3 loops did not affect the interface volumes between Ig-2D1 and 09HA and 09HA_mut significantly: 5155.2 ± 12.7 Å and 5382.0 ± 15.7 Å, respectively. This result suggests that key structural changes occurred on the antibody Ig-2D1 L1 and L3 loops.

Destabilization of the K158 salt bridge in 09HA

The 09HA retained the K167-D93 salt bridge but lost the K158-D54 salt bridge found between 18HA and Ig-2D1. The ΔG contribution of K158 was estimated to be −4.4 ± 0.2 kcal/mol in the 18HA (Table 3). The K158 salt bridge was unstable in the 09HA system and did not meet the 75% occupancy threshold. Of the epitope residues, only two mutations occurred between 18HA and 09HA: S160N and V170I, respectively. As a result, the ΔG of
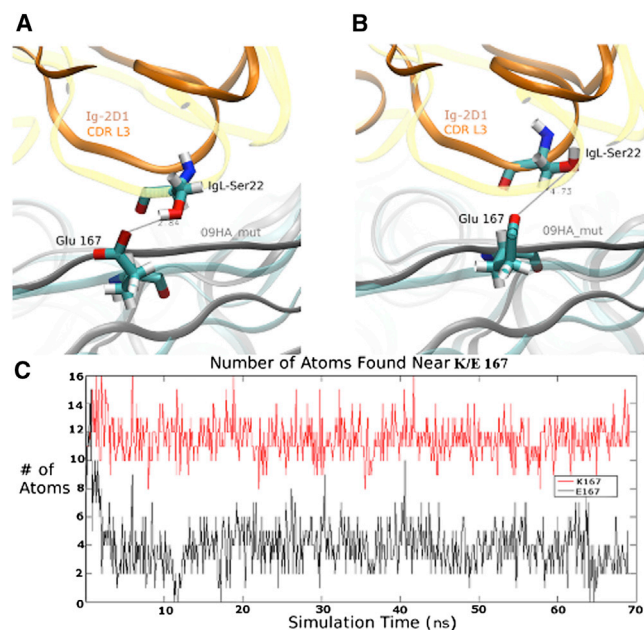

FIGURE 2 Loop motions near Glu 167 in 09HA_mut. (*A*) The position of Glu (E) 167 relative to the CDR L3 loop (*yellow*), at the beginning of the simulation. (*B*) After the end of the simulation, the loops moved away from the HA and the CDR L3 (*orange*) was further away from the Glu167. (*C*) The number of Ig-2D1 atoms (*y* axis) within 4.6 Å of K167 (09HA, *red*) and E167 (09HA_mut, *black*) over time (*x* axis). To see this figure in color, go online.

09HA and Ig-2D1 interaction increased by +6.4 ± 1.6 kcal/mol. The biggest free-energy contribution difference between 18HA and 09HA occurred at K158 and N160, with no significant differences observed from residue 161 onward (Fig. 3), including residues K167 and the V170I mutation. Thus, the difference observed at S160N may be the major mutation that affects the stability of the K158-D54 salt bridge.

S160 contributed −4.9 ± 0.2 kcal/mol to 18HA interaction with Ig-2D1, whereas N160 contributed little to the 09HA interaction with the latter (Table 3). Throughout the simulation, S160 (18HA) formed two H-bonds and two dipole-dipole interactions with Ig-2D1 (Table S2), whereas no equivalent interactions were found for N160 (09HA) (Table S3). Here we note that only one dipole-dipole interaction for S160 (18HA) is identified through crystal structure examination only, whereas all the interactions at K167 (18HA) are observed in the simulation and the crystal structure (Table S2).

We examined the volume between S160 (18HA) and N160 (09HA) and adjacent Ig-2D1 residues (Table 4). There was close to a 50% increase in the solvent-accessible volume from 18HA to 09HA. The extra volume allowed more water molecules to enter the protein interface (Fig. 4). Thus, it is likely that the S160N mutation led to increased solvent accessibility and formation of a water cavity, with a destabilizing effect on the K158-D54 salt bridge (Table S3).

Of the 20 epitope residues, the other mutation between 18 HA and 09HA is V170I. We did not find any significant interactions between HA and Ig-2D1 at position 170 during our simulations (Tables S2 and S3). Overall, the S160N could be a major contributing factor to the lower binding affinity of 09HA by Ig-2D1, in conjunction with the loss of the K158-D54 salt bridge.

Compared with 18HA, 06HA also lost the K158-D54 salt bridge with Ig-2D1. The K158 (06HA) contributed similarly to the K158 (09HA) but only half as much as the K158 (18HA) to the ΔG of Ig-2D1 binding. However, 10 additional mutations in the epitopes of 06HA resulted in a similar ΔG as 09HA overall (Tables 3 and S8). Of these, L161 (06HA) lowered ΔG from the VDW interaction with R97 (IgH) (Fig. S1). It contributed −4.0 kcal/mol ± 0.1kca/mol compared with
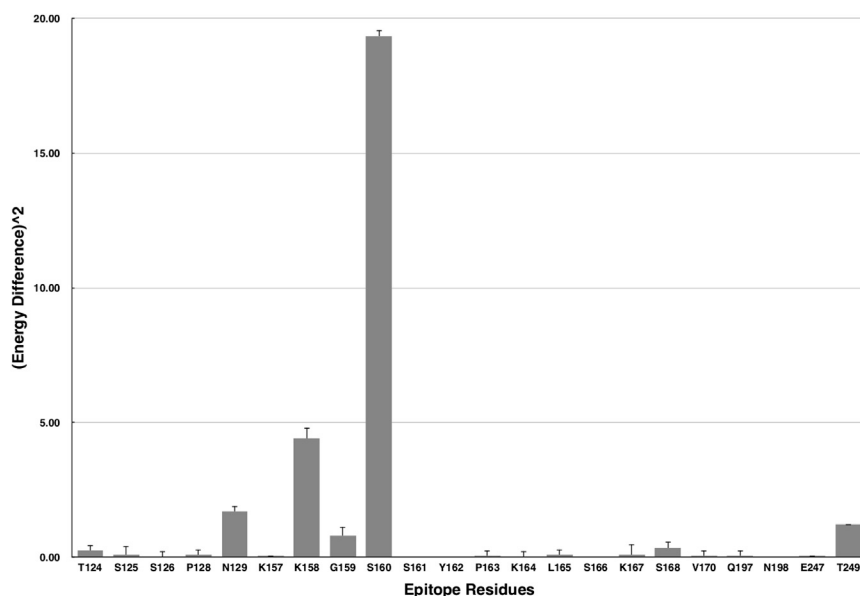
FIGURE 3 The free energy differences squared are shown for all epitope residues between 18HA and 09HA. Y axis is the energy difference squared, $\Delta\Delta G^2=(\Delta G_{18HA}-\Delta G_{09HA})^2$, and x axis are the residue name and residue ID from 18HA. The two mutations are S160N and V170I from 18HA to 09HA. Detailed data may be found in Tables 3 and S8.

1.8kcal $\pm$ 0.1kcal/mol from S161 (18HA) (Table 3). This decrease of -2.2 kcal/mol $\pm$ 0.1kcal/mol in ΔG suggests that the S161L mutation from a polar amino acid to a hydrophobic residue is favorable within the context of all the other compensatory mutations in 06HA.

DISCUSSION

Role of salt bridges on the stability of the antigen-antibody complex

In an earlier study, Krause et al. reported that Ig-2D1 against 18HA may cross-react with 09HA and identified the K167E mutation from experimental screening for escape mutants to Ig-2D1. These escape mutants are no longer neutralized by the Ig-2D1 antibody. We obtained results consistent with these experimental observations through MD simulation. The 09HA_mut had the lowest binding affinity to Ig-2D1 (Table 2). In addition, residue-based, free-energy decomposition also confirmed that K167 is a key residue in the binding of Ig-2D1.

Others have similarly predicted the importance of this residue using hot-spot analysis (21). Xu et al. determined from crystal structural and experimental mutation studies that the K167 plays a key role in forming a salt bridge between Ig-2D1 and 18HA (12,14). When K167 was mutated to E, Q, or P, the dissociation constant K_d drastically increased. As these studies are based on crystal structures alone or single-residue mutagenesis, they offer limited

mechanistic insights on how K167 affects antigen-antibody interactions.

K167 (09HA) is a positively charged amino acid residue that forms a salt bridge with negatively charged D93 (IgL). When it is mutated to E167 (09HA_mut), the two negative amino acid residues, E167 and D93, were thermodynamically unstable close together. In our MM-PB/GBSA results, the 09HA_mut bound only half as strongly as 18HA to Ig-2D1 with a ΔG of -37.9 ± 1.6 kcal/mol. Since 09HA_mut is not expected to bind, or binds poorly, to Ig-2D1, the negative ΔG could be because of the experimental setup of the simulation. The 09HA_mut system bound to Ig-2D1 was constructed artificially by superimposing the 09HA_mut and 18HA/Ig-2D1 co-crystal structures (12). Consequently, 09HA_mut was placed in close proximity to Ig-2D1, a state that may not occur in nature because of entropic barriers.

Over the length of the simulation, Ig-2D1 remained bound to 09HA_mut, with a number of favorable antigen/antibody interactions that the mutant model inherited from its 18HA/Ig-2D1 crystallographic template. However, the electrostatic repulsion between E167 and D93 eventually led to the loss of other favorable interactions between the antigen and the antibody (Table 1). In particular, two H-bond interactions were lost and not replaced between the 09HA and 09HA_mut systems.

Relative binding affinities of Ig-2D1 to HAs

Krause et al. reported that the Ig-2D1 concentration taken to neutralize 09HA is 0.04 μg/ml compared with 0.025 μg/ml required for 18HA, suggesting that the binding affinity of Ig-2D1 to 09HA is lower (14). In contrast, Liu et al. (21) predicted, using a single-frame reconstructed antigen-antibody system, that six mutations on the 09HA could help the antigen to bind more strongly to Ig-2D1. Our

TABLE 4 POVME volumes of 18HA and 09HA surrounding S/N160

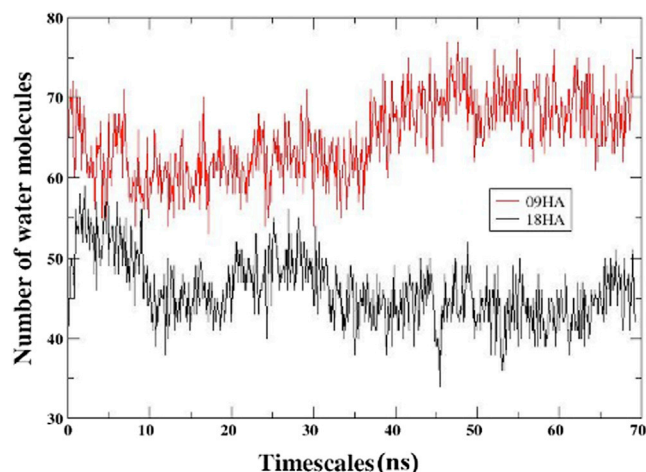|	18HA	09HA
Volume (Å³)	1317.2	1922.9
SE (Å³)	13.6	17.7

FIGURE 4 The S160N mutation and water pocket formation. The number of water molecules within 5 Å of 18HA S160 (*black*) and 09HA N160 (*red*) as a function of simulation time. To see this figure in color, go online.

simulations determined that the 09HA had weaker binding affinity with Ig-2D1, compared with 18HA, in agreement with the results of Krause et al.

Liu et al. (21) did not identify a role for N160 in the interaction between 09HA and Ig-2D1. Our free-energy decomposition analysis revealed that S160 in 18HA contributed more to binding than N160 in 09HA. Relatively speaking, the S160N mutation weakened the interaction between Ig-2D1 and HA.

The S160N mutation could destabilize the K158-D54 (IgH) salt bridge in the simulations by increasing solvent accessibility and formation of water pockets. This may be because of the loss of hydrogen bonds established by S160 from 18HA in 09HA. Even though S and N are polar amino acid residues, we did not observe any persistent H bonds or other interactions with N160 in 09HA (Table S5). The increased water present in the antibody-antigen interface could further weaken the electrostatic interactions from the salt bridges formed. Thus, the S160N mutation is likely to have a destabilizing effect on the K158-D54 salt bridge important in the antigen-antibody complex formation. This result also suggests that the antibody may be recognizing a spatial conformation presented by S160, but not N160.

In summary, Ig-2D1 has a higher ΔG toward 09HA compared with its native 18HA antigen primarily because of a S160N mutation and its secondary effects. This conclusion demonstrates the advantages of MD simulation, which allows the antigen to change, based on antibody dynamics, and represents a more realistic physiological setting.

The 09HA had only two mutations compared with the 18HA in the epitopes, of which S160N allowed partial escape from the cross-reactive 18HA antibody Ig-2D1. The 06HA, with 10 mutations in the epitope residues, was still recognized by Ig-2D1 at a similar affinity as the

09HA in silico. Next we discuss how the 06HA might be able to escape from Ig-2D1 immune recognition in vivo.

Effect of glycosylation on 06HA recognition

The ΔGs of the 06HA and 09HA systems were -67.6 ± 1.6 kcal/mol and -68.0 ± 1.2 kcal/mol, respectively. However, 06HA is not neutralized by Ig-2D1 experimentally. Our sequence analysis revealed that this is likely because of mutations in 06HA that introduce glycosylation in vivo, which provides the necessary immune escape (Fig. 1 *B*). K164 from the 18HA is mutated to N164 in the 06HA. This K164N mutation introduced a glycosylation site on the Sa epitope. Another E131T mutation added a glycosylation site at position 129.

Glycosylation has been suggested as a defense mechanism against antibody neutralization (5,19,39). The carbohydrates attached on epitopes cause steric crash with antibodies. In our simulation, the 06HA system was unglycosylated. During system setup, all carbohydrates were removed. Thus, the Sa epitope was exposed to Ig-2D1 without any steric hindrance. The ΔG free-energy calculation results suggest Ig-2D1 could neutralize the unglycosylated 06HA.

Thus, the in-silico experimental construct allowed Ig-2D1 to bind/neutralize the 06HA even though it may not be feasible under physiological conditions where glycosylation is present. We cannot exclude other mechanisms in play here, because there are more mutations of 06HA among the epitope residues. For example, in this case, spatial conformations may be more important in epitope recognition by Ig2-2D1. Nonetheless, our observations suggest a mechanism for immune augmentation through which glycosylation inhibitors may enhance protection from preexisting antibodies or immune memory.

MM-PB/GBSA analysis for relative binding-energy determination

The PB model for implicit solvent was considered more accurate than the GB method for free-energy calculations (40). However, recent research has shown that the GB implicit-solvent model may be better at predicting relative binding energy than the PB model (41). In the current work, both the GB and PB models performed similarly, as judged by the relative ΔG rankings of the four HA/Ig-2D1 systems studied (Table 2). MM-PBSA is relatively fast and could predict relative binding energy very well (42), and our results provided further support for the validity of MM-PBSA in the antibody-antigen systems studied. Other methodologies have been reported in the literature to calculate the free energy of binding, including free-energy perturbation (FEP) and thermodynamic integration (TI) (43,44). Even though both of these methods can produce ΔG values

that closely match experiment values, they are computationally more expensive.

Xia et al. used FEP to determine the $\Delta\Delta G$s between different HAs and monoclonal antibodies. Their results showed that a single escape mutation would increase the $\Delta\Delta G$ by 7.28–15.47 kcal/mol (43). Interestingly, our decomposition energy also showed that the K167E mutation contributed 9.2 ± 0.3 kcal/mol to the total ΔG of the 09HA_mut system. Since ΔG calculation with MM-PB/GBSA for a salt bridge is often overestimated if the salt bridge is buried between two protein interfaces (45), the $+9.2 \pm 0.3$ kcal/mol difference in energy could be the upper-bound limit. Other residues that Xia et al. suggested would change binding affinity without being detrimental to antibody-antigen interactions had reported $\Delta\Delta G$ values <4.24 kcal/mol. Our results also predicted that, for mutations that do not reverse binding, their $\Delta\Delta G$s in decomposition energies were also <2.2 kcal/mol.

Entropy consideration in relative binding-energy determination

Conformational entropy has been implicated in the antibody maturation process when mutations in the Fab and Fc regions modulate the binding of antibodies to antigens (46). In our simulation, we did not consider entropic contributions in our specific systems for several reasons. First, the systems are similar in their binding states, as shown through RMSD analyses. HA receptor-binding domains are very rigid: only side-chain movements were observed. Second, no major conformational changes were observed in the antibody or antigen. This observation is in contrast to that of our previous study in which glycan receptors adopted significant changes upon HA binding, and entropy consideration was necessary to obtain results consistent with experimental studies (46).

Third, because we are considering the relative free energy of binding of complexes between highly conserved HAs and the same antibody, it is likely that the entropic differences would cancel out. Hou et al. discussed in detail that the inclusion of entropy consideration is not predictive of accuracy in all systems when relative ΔG ($\Delta\Delta G$) is calculated. In fact, many previous studies have ranked relative affinities of ligands successfully without entropy consideration (41). However, this does not mean entropy considerations may be ignored for relative binding affinities, as shown in (46). It is especially crucial when absolute binding energy is considered (41).

Fourth, entropy consideration is computationally costly using nmode, and the margin of error may fluctuate widely depending on the choice of frames used in the calculations. Convergence is often an issue when using quasiharmonic analysis (48), especially given the sizes of our systems (data not shown). Therefore, the inclusion of entropic consideration may improve the correlation with experimental data, but it is beyond the scope of our current hypotheses.

CONCLUSIONS

Our computational results from MM-GB/PBSA are consistent with experimental observations reported in the literature. The formation of two salt bridges plays a key role in the immune recognition of Ig-2D1 of the 18HA and cross-reactivity with the 09HA. The stability of the K158-D54 (IgH) salt bridges is dramatically weakened by the S160N mutation in the 09HA and is accompanied by hydrogen bond loss and water pocket formation at the antibody-antigen interface. The immune escape of the 09HA may be accomplished through a K167E mutation, which completely disrupts both salt bridges between 09HA and Ig-2D1. On the other hand, the 06HA likely achieves immune escape through mutations that introduce glycosylation sites and mask epitope residues. These results provide mechanistic insights into the immune recognition and escape of the H1N1 virus. In addition, they could inform the design of better antibodies against this pandemic strain and protection from future threats.

SUPPORTING MATERIAL

One figure and eight tables are available at http://www.biophysj.org/biophysj/supplemental/S0006-3495(15)00406-3.

AUTHOR CONTRIBUTIONS

P.I., R.E.A., and W.W.L. designed the experiments; P.I. executed the experiments; P.I., R.E.A., W.W.L. analyzed the data; and P.I., R.E.A., and W.W.L. wrote the manuscript.

ACKNOWLEDGMENTS

REFERENCES

1. Rossman, J. S., and R. A. Lamb. 2011. Influenza virus assembly and budding. *Virology.* 411:229–236.

2. Nicholls, J. M., R. W. Chan, …, J. S. Peiris. 2008. Evolving complexities of influenza virus and its receptors. *Trends Microbiol.* 16:149–157.

3. Schwarzer, J., E. Rapp, …, U. Reichl. 2009. Glycan analysis in cell culture-based influenza vaccine production: influence of host cell line and virus strain on the glycosylation pattern of viral hemagglutinin. *Vaccine.* 27:4325–4336.

4. Vanderlinden, E., and L. Naesens. 2013. Emerging antiviral strategies to interfere with influenza virus entry. *Med. Res. Rev.* 34:301–339.

5. Wang, C. C., J. R. Chen, …, C. H. Wong. 2009. Glycans on influenza hemagglutinin affect receptor binding and immune response. *Proc. Natl. Acad. Sci. USA.* 106:18137–18142.

6. Lachmann, P. 2009. Anti-infective antibodies—reviving an old paradigm. *Vaccine.* 27 (*Suppl. 6*):G33–G37.

7. Townsend, K. A., and L. S. Eiland. 2006. Combating influenza with antiviral therapy in the pediatric population. *Pharmacotherapy.* 26:95–103.

8. Wrammert, J., K. Smith, …, P. C. Wilson. 2008. Rapid cloning of high-affinity human monoclonal antibodies against influenza virus. *Nature.* 453:667–671.

9. Skehel, J. J., and D. C. Wiley. 2000. Receptor binding and membrane fusion in virus entry: the influenza hemagglutinin. *Annu. Rev. Biochem.* 69:531–569.

10. Gerhard, W., J. Yewdell, …, R. Webster. 1981. Antigenic structure of influenza virus haemagglutinin defined by hybridoma antibodies. *Nature.* 290:713–717.

11. Igarashi, M., K. Ito, …, A. Takada. 2010. Predicting the antigenic structure of the pandemic (H1N1) 2009 influenza virus hemagglutinin. *PLoS ONE.* 5:e8553.

12. Xu, R., D. C. Ekiert, …, I. A. Wilson. 2010. Structural basis of preexisting immunity to the 2009 H1N1 pandemic influenza virus. *Science.* 328:357–360.

13. Ekiert, D. C., R. H. Friesen, …, J. Goudsmit. 2011. A highly conserved neutralizing epitope on group 2 influenza A viruses. *Science.* 333: 843–850.

14. Krause, J. C., T. M. Tumpey, …, J. E. Crowe, Jr. 2010. Naturally occurring human monoclonal antibodies neutralize both 1918 and 2009 pandemic influenza A (H1N1) viruses. *J. Virol.* 84:3127–3130.

15. Wrammert, J., D. Koutsonanos, …, P. C. Wilson. 2011. Broadly cross-reactive antibodies dominate the human B cell response against 2009 pandemic H1N1 influenza virus infection. *J. Exp. Med.* 208:181–193.

16. Ping, J., L. Keleta, …, E. G. Brown. 2011. Genomic and protein structural maps of adaptive evolution of human influenza A virus to increased virulence in the mouse. *PLoS ONE.* 6:e21740.

17. Khiabanian, H., V. Trifonov, and R. Rabadan. 2009. Reassortment patterns in Swine influenza viruses. *PLoS ONE.* 4:e7366.

18. World Health Organization. 2009. http://www.who.int/mediacentre/news/statements/2009/h1n1_pandemic_phase6_20090611/en/index.html. Accessed December 28, 2011.

19. Hancock, K., V. Veguilla, …, J. M. Katz. 2009. Cross-reactive antibody responses to the 2009 pandemic H1N1 influenza virus. *N. Engl. J. Med.* 361:1945–1952.

20. Itoh, Y., K. Shinya, …, Y. Kawaoka. 2009. In vitro and in vivo characterization of new swine-origin H1N1 influenza viruses. *Nature.* 460:1021–1025.

21. Liu, Q., S. C. H. Hoi, …, J. Li. 2011. Structural analysis of the hot spots in the binding between H1N1 HA and the 2D1 antibody: do mutations of H1N1 from 1918 to 2009 affect much on this binding? *Bioinformatics.* 27:2529–2536.

22. Whittle, J. R., R. Zhang, …, S. C. Harrison. 2011. Broadly neutralizing human antibody that recognizes the receptor-binding pocket of influenza virus hemagglutinin. *Proc. Natl. Acad. Sci. USA.* 108:14216–14221.

23. Pettersen, E. F., T. D. Goddard, …, T. E. Ferrin. 2004. UCSF Chimera—a visualization system for exploratory research and analysis. *J. Comput. Chem.* 25:1605–1612.

24. Maestro, version 9.3. Schrödinger, New York.

25. Hornak, V., R. Abel, …, C. Simmerling. 2006. Comparison of multiple Amber force fields and development of improved protein backbone parameters. *Proteins.* 65:712–725.

26. Li, H., A. D. Robertson, and J. H. Jensen. 2005. Very fast empirical prediction and rationalization of protein pKa values. *Proteins.* 61:704–721.

27. Dolinsky, T. J., P. Czodrowski, …, N. A. Baker. 2007. PDB2PQR: expanding and upgrading automated preparation of biomolecular structures for molecular simulations. *Nucleic Acids Res.* 35:W522–W525.

28. Phillips, J. C., R. Braun, …, K. Schulten. 2005. Scalable molecular dynamics with NAMD. *J. Comput. Chem.* 26:1781–1802.

29. Jorgensen, W. L., J. Chandrasekhar, …, M. L. Klein. 1983. Comparison of simple potential functions for Simulating liquid water. *J. Chem. Phys.* 79:926–935.

30. Barlow, D. J., and J. M. Thornton. 1983. Ion-pairs in proteins. *J. Mol. Biol.* 168:867–885.

31. Marqusee, S., and R. L. Baldwin. 1987. Helix stabilization by Glu-…Lys+ salt bridges in short peptides of de novo design. *Proc. Natl. Acad. Sci. USA.* 84:8898–8902.

32. Humphrey, W., A. Dalke, and K. Schulten. 1996. VMD: visual molecular dynamics. *J. Mol. Graphics.* 14:33–38.

33. Miller, B. R., T. D. McGee, …, A. E. Roitberg. 2012. *MMPBSA.py*: an efficient program for end-state free energy calculations. *J. Chem. Theory Comput.* 8:3314–3321.

34. Case, D. A., T. E. Cheatham, 3rd, …, R. J. Woods. 2005. The Amber biomolecular simulation programs. *J. Comput. Chem.* 26:1668–1688.

35. Onufriev, A., D. Bashford, and D. A. Case. 2004. Exploring protein native states and large-scale conformational changes with a modified generalized born model. *Proteins.* 55:383–394.

36. Amaro, R. E., X. Cheng, …, J. A. McCammon. 2009. Characterizing loop dynamics and ligand recognition in human- and avian-type influenza neuraminidases via generalized born molecular dynamics and end-point free energy calculations. *J. Am. Chem. Soc.* 131:4702–4709.

37. Sievers, F., A. Wilm, …, D. G. Higgins. 2011. Fast, scalable generation of high-quality protein multiple sequence alignments using Clustal Omega. *Mol. Syst. Biol.* 7:539.

38. Durrant, J. D., L. Votapka, …, R. E. Amaro. 2014. POVME 2.0: an enhanced tool for determining pocket shape and volume characteristics. *J. Chem. Theory Comput.* 10:5047–5056.

39. Binley, J. M., Y. E. Ban, …, R. W. Sanders. 2010. Role of complex carbohydrates in human immunodeficiency virus type 1 infection and resistance to antibody neutralization. *J. Virol.* 84:5637–5655.

40. Feig, M., A. Onufriev, …, C. L. Brooks, 3rd. 2004. Performance comparison of generalized born and Poisson methods in the calculation of electrostatic solvation energies for protein structures. *J. Comput. Chem.* 25:265–284.

41. Hou, T., J. Wang, …, W. Wang. 2011. Assessing the performance of the MM/PBSA and MM/GBSA methods. 1. The accuracy of binding free energy calculations based on molecular dynamics simulations. *J. Chem. Inf. Model.* 51:69–82.

42. Lee, V. S., P. Tue-ngeun, …, C. Tayapiwatana. 2010. Pairwise decomposition of residue interaction energies of single chain Fv with HIV-1 p17 epitope variants. *Mol. Immunol.* 47:982–990.

43. Xia, Z., T. Huynh, …, R. Zhou. 2012. Free-energy simulations reveal that both hydrophobic and polar interactions are important for influenza hemagglutinin antibody binding. *Biophys. J.* 102:1453–1461.

44. Gouda, H., I. D. Kuntz, …, P. A. Kollman. 2003. Free energy calculations for theophylline binding to an RNA aptamer: comparison of MM-PBSA and thermodynamic integration methods. *Biopolymers.* 68:16–34.

45. Huo, S., I. Massova, and P. A. Kollman. 2002. Computational alanine scanning of the 1:1 human growth hormone-receptor complex. *J. Comput. Chem.* 23:15–27.

46. Corrada, D., and G. Colombo. 2013. Energetic and dynamic aspects of the affinity maturation process: characterizing improved variants from the bevacizumab antibody with molecular simulations. *J. Chem. Inf. Model.* 53:2937–2950.

47. Reference deleted in proof.

48. Xu, D., E. I. Newhouse, …, P. W. Arzberger. 2009. Distinct glycan topology for avian and human sialopentasaccharide receptor analogues upon binding different hemagglutinins: a molecular dynamics perspective. *J. Mol. Biol.* 387:465–491.

49. Reference deleted in proof.